Proc. Indian Acad. Sci. (Earth Planet. Sci.), Vol. 95, No. 2, July 1986, pp. 209–221.

Physico-chemical conditions of ore deposition in Malanjkhand copper sulphide deposit

S JAIRETH and M SHARMA
Department of Earth Sciences, University of Roorkee, Roorkee 247 667, India

MS received 27 April 1985; revised 6 November 1985

Abstract. Heating and freezing studies on fluid inclusions in quartz from mineralized quartz-feldspar reef reveal the presence of type A $CO_2 - H_2O$ ($H_2O > 50\%$ by volume), type B $CO_2 - H_2O$ ($H_2O < 50\%$ by volume), type C pure CO_2 and type D pure aqueous inclusions. Types A, B and C are primary and/or psuedo-secondary inclusions while type D are secondary. Types A and B homogenize on heating into different phases at similar temperatures ranging between 307 and 476 °C, indicating entrapment from boiling hydrothermal solutions. Type D inclusions homogenize into a liquid phase at temperatures between 88 and 196 °C. Boiling of hydrothermal solutions led to the formation of a CO_2-rich phase of low density and salinity that coexisted with another dense and saline aqueous phase with very little CO_2 dissolved in it. Ore and gangue mineral assemblage of primary ores indicate that ore deposition was characterized by $\log f_{O_2} = -34{\cdot}4$ to $-30{\cdot}2$ atm, $\log f_{S_2} = -11{\cdot}6$ to $-8{\cdot}8$ atm and pH = 4·5 to 6·5.

Keywords. Fluid inclusion; homogenization; boiling; fugacity.

1. Introduction

The Malanjkhand copper sulphide deposit is situated near Padritola, Baihar Tehsil, Balaghat district of Madhya Pradesh. Sharma and Kumar (1969) worked out the stratigraphic sequence of rocks of the area. Rao (1974) carried out ore microscopic studies and proposed a paragenetic sequence of ore-forming minerals. Narang *et al* (1979) discussed factors controlling ore localization while Tripathi (1979) found enough evidence to name Malanjkhand a copper porphyry deposit. Earlier attempts to understand the physico-chemical conditions of ore deposition are few and controversial. Rao (1974), who studied ore paragenesis indicated very high temperatures (450 to 700°C) of ore formation. Sharma (1982), based on the analysis of relevant $\log f_{O_2} - \log f_{S_2}$ diagrams for mineral assemblages in ores, indicated equally high temperatures (307 to 547 °C) of ore formation. In the present work, detailed fluid inclusion studies have been undertaken to establish physico-chemical (temperature, pressure, physical and chemical nature of mineral forming media, etc) conditions of ore deposition.

2. Geological setting

Archean granite-granodiorite are the main rocks of the area. These have been intruded by a number of basic dykes and are overlain unconformably by younger metasedimentaries of Chilpi Ghat series represented by conglomerates, arkosic grits, quartzites and phyllites. The metasedimentaries have a general ENE-WSW trend with dips of 30 to 50° due SSE (Rao 1974).

The most conspicuous geological element in the area is a quartz-feldspar reef occupying a shear zone within granite-granodiorite. The quartz reef is arcuate in shape (see figure 1) with its convexity directed towards east. Strike direction of the reef changes from NNW–SSE in the northern to N–S in the central and NE–SW in the southern parts of the area. The reef is about 10 to 30 m thick and dips steeply (60° to 70°) due east in the central part.

According to Sharma (1982), within the suite of granite-granodiorite rocks, granodiorite is the most dominant type. Tonalite and quartz-monzonite are present in lesser amounts.

Copper mineralization is confined mainly to the quartz-feldspar reef and has been traced to a strike length of $\simeq$ 1100 m. Mineralization persists to depths greater than 200 to 300 m. Within the reef, mineralization is irregular, distributed mainly as disseminations, stringers and pockets. Chalcopyrite is the main mineral of primary ores followed by pyrite and magnetite. Molybdenite, sphalerite and cobaltite are present in minor amounts. At places, molybdenite forms relatively richer pockets within the reef. Primary sulphide ores are capped by zones of oxidation and secondary enrichment. Thickness of supergene zones varies from 100 to 110 m with maximum in the southern block of the ore deposit. Malachite, azurite, goethite, bornite, chalcocite, covellite and native copper are the main minerals of supergene zones.

Primary sulphide mineralization is accompanied by intensive wall rock alteration of granite-granodiorite rocks manifested in the development of pink feldspar, biotite, epidote, chlorite, sericite and kaolinite.

3. Types of fluid inclusions

Fifteen polished plates of quartz from the mineralized quartz-feldspar reef were studied using a normal polarized light microscope. Fluid inclusions in quartz are generally very small ($<$ 20–25 μm) which makes their study rather difficult. Optical microscopy coupled with heating and freezing studies have helped to identify the following basic types of fluid inclusions in quartz: (i) Type A, CO_2–H_2O inclusions ($H_2O > 50\%$ by volume); (ii) Type B, CO_2–H_2O inclusions ($H_2O < 50\%$ by volume); (iii) Type C, CO_2 inclusions and (iv) Type D, aqueous inclusions.

Type A inclusions are characterized by sharp and regular cavity boundaries. Few of these have typical negative crystal shapes. These inclusions are distributed at random within one grain or form small bands cutting across one or more grains (see figure 2). Both the distribution pattern and the inclusion shape suggest that they are primary and/or psuedo-secondary inclusions.

At room temperature these inclusions contain a gas bubble (10–30% by volume of the cavity) but slight cooling below the room temperature nucleates a separate phase of liquid CO_2 occupying the interface between gaseous phase (CO_2) and aqueous phase. Some type A inclusions locally contain opaque and/or isotropic solid but such inclusions are extremely rare.

Type B inclusions at room temperature contain a gas bubble ($<$ 50% by volume of the cavity), but slight cooling below room temperature, nucleates a separate phase of liquid CO_2. In shape and pattern of distribution, these inclusions are similar to type A inclusions and occupy the same clusters of random inclusion or constitute the same bands of inclusions (see figure 2).

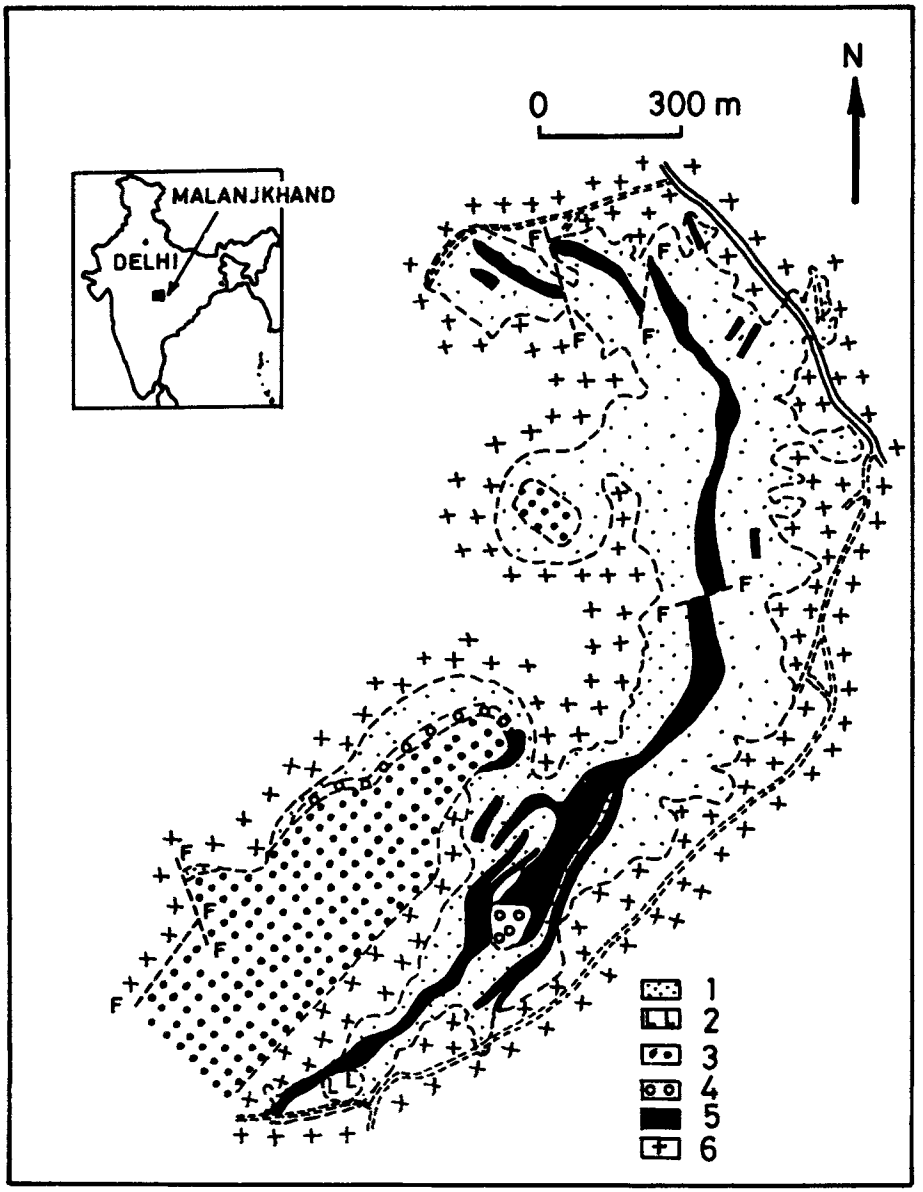

Figure 1. Geological map of Malanjkhand copper deposit, modified after Narang *et al* (1979), 1. Talus 2. Laterite 3. Arkosic grit, quartzite and phyllite 4. Conglomerate 5. Quartz reef 6. Granite/granodiorite.

Type C inclusions at room temperature are similar to the so-called dry gaseous inclusions with CO_2 occupying the whole volume of the cavity. A thin film of aqueous phase might also be present in them. In some of these inclusions freezing nucleated a separate bubble representing gaseous CO_2. Type C inclusions are closely associated with type A and type B inclusions (see figure 2). All the three types i.e. types A,B,C are thus primary and/or pseudo-secondary inclusions, syngenetic to each other.

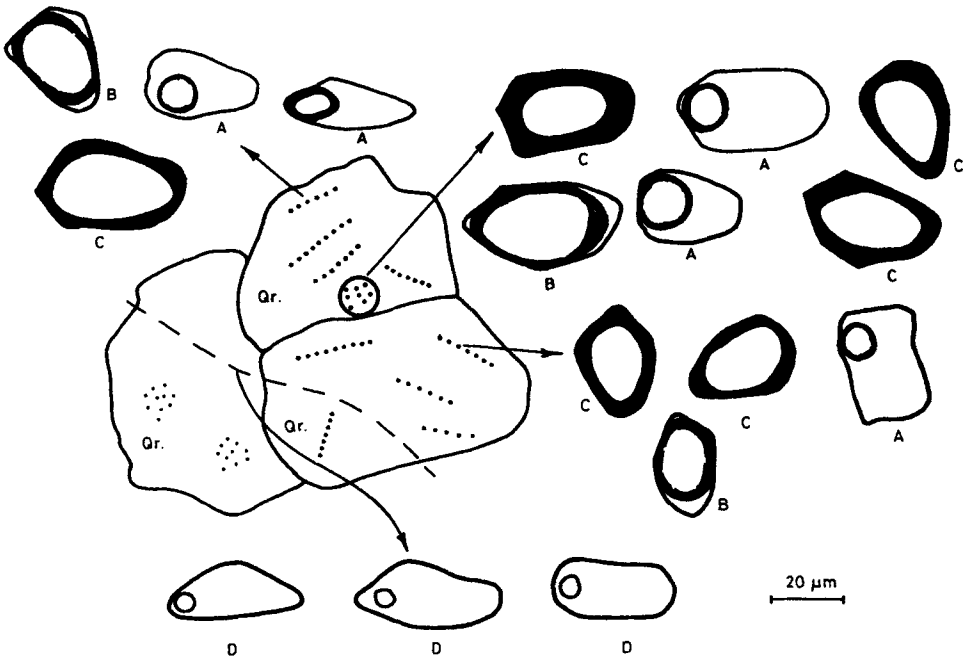

Figure 2. Schematic representation of quartz (Qr) grains showing distribution of types A,B,C and D inclusions. The dark bubble in all types A,B and C inclusions is CO_2 which is surrounded by an aqueous phase. In type D inclusions bubble is vapour surrounded by aqueous phase.

Type D inclusions contain at room temperature a gas bubble ($< 5\%$ by volume of the cavity) and are distributed as large bands cutting across large number of grains (see figure 2). They have highly irregular shapes and are thought to be formed due to healing of larger microfractures and hence are secondary. These inclusions are free of solids and do not contain CO_2.

4. Heating studies

Selected fluid inclusions were heated in a temperature programmable Linkam TH 600 heating freezing system, calibrated carefully using calibration standards recommended by MacDonald and Spooner (1981). Inclusions having irregular cavity boundaries or showing signs of necking down were not heated. Heating was carried out at a constant rate of 10 °C/min.At temperatures closer to temperatures of homogenization, rate of heating was further reduced to 5 °C/min. Temperatures of homogenization of various types of inclusions are shown in figure 3.

All type A inclusions homogenized in two stages. In the first stage gaseous CO_2 homogenized into liquid CO_2 phase at temperatures between + 17·3 °C and + 30·4 °C (see figure 3a). It should be mentioned that heating at this stage was carried out at constant rates of 0·5 °C/min to 1 °C/min. On further heating all these inclusions homogenized into a liquid phase with the disappearance of gas bubble (CO_2 phase) at temperatures between 210 °C and 476 °C with a mean value of 289 °C obtained from

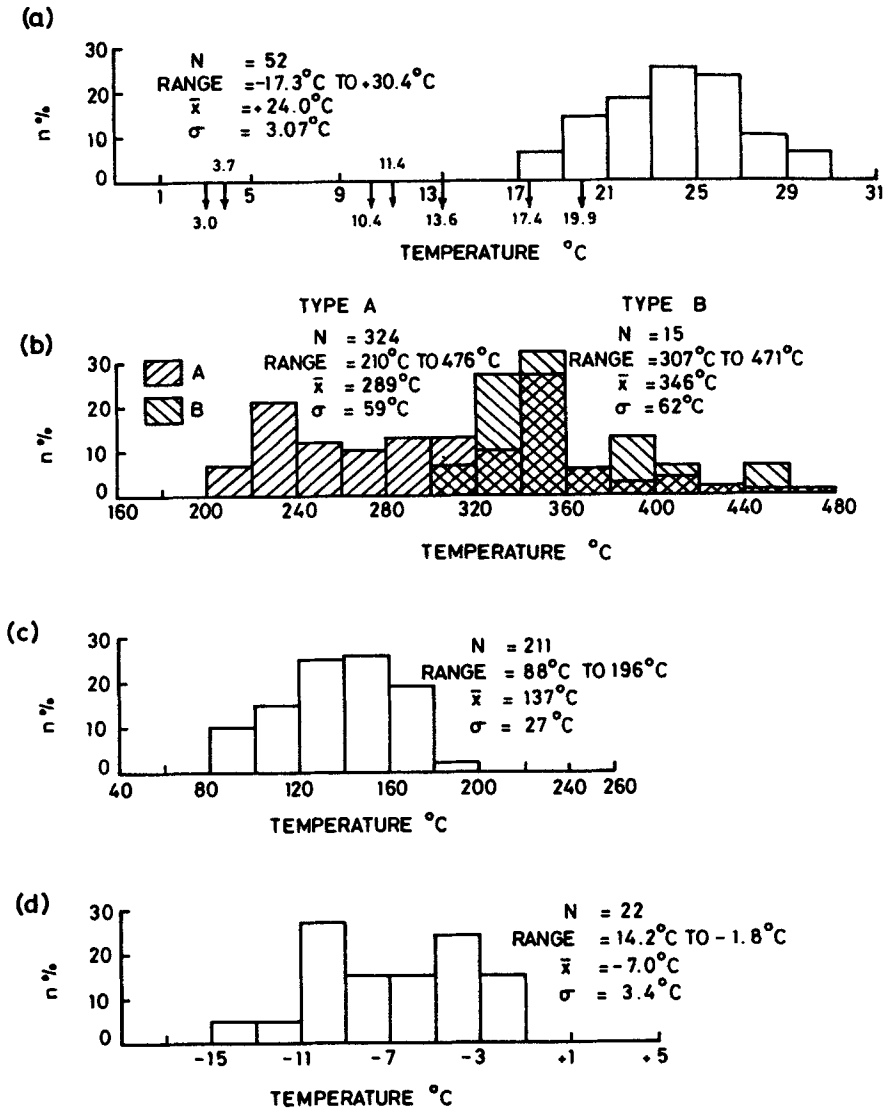

Figure 3. **a.** Temperature of homogenization of CO_2 phases of types A, B and C inclusions. Homogenization temperatures of a few type B and C inclusions are shown as inverted arrows at points corresponding to their temperatures of homogenization. In all inclusions, CO_2 phases homogenize by disappearance of gaseous CO_2. **b.** Temperature of final homogenization of primary and/or pseudo-secondary types A and B inclusions. Type A inclusions homogenize into liquid phase while type B homogenize into supercritical CO_2 fluid; **c.** Temperature of final homogenization of secondary type D inclusions. **d.** Temperature of final melting of ice in type A inclusions.

heating of 324 such inclusions (see figure 3b). In type A inclusions with solids, continuous heating beyond temperatures of disappearance of gas bubble did not lead to dissolution of solids, and the inclusions exploded. Probably, all these solids are captive solids i.e. solids entrapped along with the mineral forming aqueous solution.

All type B inclusions also homogenized in two stages. First, at temperatures between

+ 3·0 °C and + 19·9 °C, CO_2 phase became homogeneous with the gradual disappearance of gaseous CO_2 (see figure 3a). On further heating, dark bubble (CO_2 phase) gradually expanded to fill up the whole volume of the cavity at temperatures of homogenization varying between 307 and 471°C, with a mean value of 360°C obtained from 15 such inclusions (see figure 3b).

Secondary type D inclusions homogenized into liquid phase at temperature between 83 and 196°C with a mean value of 137°C obtained from 211 such inclusions (see figure 3c).

5. Freezing studies

Freezing studies were carried out on a Linkam TH 600 heating-freezing system to determine the composition, and salinity of entrapped material. Before freezing, the stage was calibrated using distilled water (melting point = 0 °C) and *n*-octane (melting point = − 56·6 °C) sealed in flat bottomed capillary tubes as standards. Inclusions were first frozen and phase changes were observed during gradual warming.Heating rate close to the expected points of phase changes was kept as low as 0·1 °C/min and 0·5 °C/min.

The liquid in type A inclusions usually froze at temperatures between − 40 and − 60 °C. Accurate recording of the temperature of first melting (temperature of eutectic) is normally difficult and therefore repeated freezing runs were undertaken to determine this temperature as accurately as possible.

Liquid CO_2 in types A, B and C inclusions showed considerable resistance to solidification particularly in types B and C inclusions. Considerable overcooling (upto − 130 °C) was required to solidify liquid CO_2 in these inclusions. In types A, B and C inclusions, freezing first produced a small bubble separating gaseous CO_2 from liquid CO_2 followed by solidification of liquid CO_2 at considerably low temperatures. Formation of CO_2 hydrate (Clathrate) has been observed by many workers during freezing studies on CO_2 bearing inclusions (Roedder 1963; Kelly and Turneaure 1970; Collins 1979 etc). Clathration is usually recorded with the help of double freezing of such inclusions (Collins 1979), where clathrate freezes out first followed by freezing of aqueous phase. In types A, B and C inclusions despite appreciable amount of detectable CO_2 phase, we have not been able to identify clathration. It might be possible that because of the small size of these inclusions (< 20–25 μm) it was difficult to observe double freezing. Further, in many type B inclusions, the amount of aqueous phase was probably too small to form detectable amounts of clathrate. It should be mentioned that clathration has not been detected in many other CO_2 bearing fluid inclusions from other localities (Luckscheiter and Morteani 1980). Heating and freezing data on all types of fluid inclusions are summarized in table 1.

6. Pressure and temperature conditions of ore formation

Primary sulphides, as mentioned earlier, are distributed as disseminations, small stringers and veinlets within quartz-feldspar reef. Textural relationship between primary sulphides and gangue (quartz and orthoclase) minerals indicates that sulphides are syngenetic to the bulk of the quartz and feldspar. Hence primary and/or pseudo-

Table 1. Heating and freezing data (in °C) for types A,B,C and D inclusions in quartz.

Type of inclusions	T_m CO_2	T_e	T_m ice	T_h $CO_{2\,V-L}$	T_{hV-L}
A	−56·0 to −56·4	−22·4 to −23·4	−14·2 to −1·8	+17·3 to +30·4	210 to 476 (L)
B	−56·0 to −56·4	nd	nd	+ 3·0 to +19·9	307 to 471 (CO_2)
C	−56·0 to −56·4	nd	nd	+ 3·7 and +15·6	nd
D	—	nd	nd	—	88 to 196 (L)

T_m Temperature of melting; T_e Temperature of first melting i.e. temperature of eutectic; T_h $CO_{2\,V-L}$ Temperature of homogenization of CO_2 phases; T_{hV-L} Temperature of final homogenization. Letters in brackets represent final phase of homogenization; V-Vapour/gas; L-Liquid; nd-not determined

secondary types A, B and C inclusions observed in quartz, represent mineral-forming solutions responsible for the main episode of ore formation. Secondary type D inclusions are either related to the same mineralization episode or represent any later hydrothermal event superimposed on it.

6.1 *Boiling*

As mentioned earlier types A, B and C inclusions which show highly variable CO_2/H_2O ratio occupy the same clusters of random inclusions or constitute the same bands of inclusions (see figure 2) indicating that these inclusions are syngenetic to each other. In addition, these inclusions homogenize into different phases (type A into liquid and type B into gaseous) at almost similar temperatures (see figure 3) suggesting that entrapment of these inclusions took place from heterogeneous mineral-forming solutions caused by boiling. Entrapment of different amounts of the immiscible fractions of the boiling solutions resulted in the formation of syngenetic inclusions showing large variation of CO_2/H_2O ratio. Large variation in the temperature of their final homogenization also supports this suggestion (Ramboz *et al* 1982). Heterogeneous entrapment i.e. boiling is also indicated by considerable variation of the homogenization temperatures of CO_2 phases in these inclusions (see figure 3a).

Experimental studies of H_2O–CO_2 system reveal an immiscibility solvus, with solvus crest at 275 °C (at 1 kbar) for pure CO_2 and H_2O mixture (Todheide and Frank 1963 in Hollister 1981). Addition of electrolytes to the mixtures greatly expands the region of immiscibility (Takenouchi and Kennedy 1965). For 6 wt % salt in the aqueous phase, solvus crest rises to about 420 °C at 1·5 kbar (Gehrig *et al* 1969 cited in Hollister 1981). In the case of Malanjkhand ores, CO_2-rich saline solutions underwent immiscibility due to boiling, generating almost pure supercritical CO_2 coexisting with relatively CO_2-poor aqueous solution. Entrapment of mixed proportions of the two immiscible fluids generated inclusions showing large variation in temperatures of homogenization.

6.2 *Composition and salinity of solutions*

Freezing studies of type A inclusions show that solids within these inclusions start dissolving at temperatures between −22·9°C and −23·9°C (table 1). This temperature,

Table 2. Concentration of CO_2 and Bulk molar volumes of entrapped media in Types A and B inclusions.

Type	Vol % H_2O at 40 °C*	Temperature of homogenization (Th $CO_{2\ V-L}$) °C	Bulk molar volume (cm^3/mole)**	Concentration of CO_2 (mole %)**
A	90	+17·3	20·8	2
A	80	+30·4	22·2	5
B	40	+ 3·0	28·6	30

* Vol % of liquid phase estimated visually; ** Bulk molar volume of entrapped fluid and mole % of CO_2 determined using curves given by Burruss (1981)

/hich is known as temperature of eutectic, is sufficiently close to −22·9 °C, the eutectic temperature in NaCl–KCl–H_2O system (Crawford 1981) which means that the liquid entrapped in these inclusions was sufficiently rich in chlorides of sodium and potassium.

Usually, salinities of aqueous phase in the fluid inclusions are determined using depression of the fusion temperature of ice recorded during freezing of these inclusions. But in all those inclusions, where CO_2 phase is also present, formation of clathrate makes residual aqueous phase more saline and depression of the fusion temperature of ice gives relatively higher estimates of salinities. For such inclusions Collins (1979) proposed use of the decomposition temperature of clathrate for the estimation of salinities. In type A inclusions though detectable amount of CO_2 is present (table 2), clathration could not be identified. On the other hand, temperature of fusion of ice in these inclusions varied between −14·2 °C and −1·8 °C with a mean value of −7·0 °C obtained from freezing of 22 such inclusions (see figure 3d). This corresponds to a salinity varying from 18 to 2·3 wt % equivalent of NaCl with a mean value of 10·5 wt % equivalent of NaCl (Potter *et al* 1978 in Roedder 1984). These values represent maximum salinity assuming that clathration in type A inclusions did occur but could not be identified.

6.3 *CO_2 in fluid inclusions*

As mentioned earlier quartz from the mineralized reef contains large number of mixed CO_2–H_2O and pure CO_2 inclusions. Freezing studies of these mixed CO_2–H_2O (types A and B) inclusions give temperature of melting of CO_2 varying between −56·0 °C and −56·4 °C which is close to the temperature of melting of pure CO_2 (−56·6 °C). Temperatures of homogenization of CO_2 phases in these inclusions have been used to estimate bulk molar volume and mol % of CO_2 in the entrapped fluid by taking the help of curves proposed by Burruss (1981). These data have been summarized in table 2. Thus, type B inclusions which homogenize with the disappearance of liquid phase at the final temperature of homogenization clearly have fluids of lower density, higher bulk molar volume and higher mol % of CO_2 in them. The coexisting type A inclusions that homogenize with the disappearance of gas bubble at the final temperature of homogenization are relatively more dense, and contain lesser amounts of CO_2 (2–5 mol %). These results agree with the general trend observed during immiscibility in CO_2–H_2O and CO_2 H_2O–NaCl system where CO_2 preferentially fractionates into a lower density fluid.

6.4 *Temperature of formation*

From the preceding discussion it is clear that the primary and/or pseudo-secondary inclusions of type A, type B and type C in quartz were formed from CO_2-bearing aqueous solution of NaCl and KCl, boiling during entrapment, i.e. at the time of entrapment vapour pressure of the solution was higher than the confining pressure. As a result, the temperatures of homogenization of these inclusions do not need any pressure correction and these temperatures represent true temperatures of entrapment. Hence, it can be concluded that mineralized quartz-feldspar reef was formed at temperatures between 210 °C and 476 °C from hydrothermal solutions that underwent recurrent boiling between temperatures of 307 °C and 476 °C. More precisely, boiling occurred at around 307 °C which is the lowest temperature of homogenization at which both types A and B inclusions homogenize into two different phases (type A into liquid and type B into gaseous).

6.5 *Pressure during entrapment*

Figure 4 shows a number of curves representing solubility of CO_2 in NaCl solution. These curves can be used to estimate vapour pressure of NaCl solution having different amounts of CO_2 dissolved in it.

As mentioned earlier, type A inclusions represent a fluid having a maximum CO_2 concentration of 2–5 mol % (i.e. 4·5 to 11·3 wt % CO_2) and an average salinity of

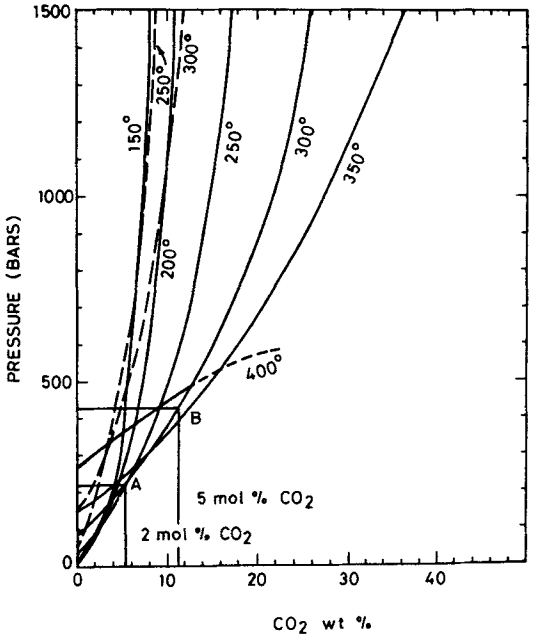

Figure 4. Diagram showing vapour pressure of CO_2 bearing NaCl solutions (modified after Takenouchi and Kennedy 1965). Thick lines are for 6 wt % NaCl solutions and dashed lines for 20 wt % NaCl solutions.

10·4 wt % equivalent of NaCl. The actual salinity, as discussed earlier, might be lower than this. Figure 4 shows that a 6 wt % NaCl solution having 2–5 mol % CO_2 and boiling at 300 °C would generate a vapour pressure of 225 to 440 bars (points A and B) respectively. These values of pressure are good approximation of pressure during entrapment of type A and syngenetic to the type B and C inclusions from boiling hydrothermal solutions. These pressures correspond to hydrostatic column depths of about 2·25 to 4·4 km or rock depths of about 1 to 2 km respectively. It should be mentioned that these values of pressure are only approximate values. Increase in salinity of the solution will bring an appreciable change in these values. For comparison, two curves for CO_2 bearing solutions of 20 wt % NaCl have also been plotted on the same figure (see figure 4). A 6 wt % NaCl solution with 5 mol % of CO_2 generates a vapour pressure of about 400 bars at 350 °C but increase in salinity upto 20 wt % NaCl enhances this pressure to about 1350 bars.

7. Geochemical parameters of ore deposition

It has been shown above that primary ore and gangue minerals were deposited from CO_2-bearing NaCl–KCl aqueous solutions that were boiling at 307°C. Hence, to estimate basic geochemical parameters (f_{O_2}, f_{S_2}, pH etc) of ore deposition a $\log f_{O_2}$–$\log f_{S_2}$ diagram at 300°C showing stability fields of main ore and gangue minerals has been calculated (see figure 5). First, a $\log f_{O_2}$–pH diagram at 300 °C was calculated using the method of Barnes and Kullerud (1961). This diagram had fields of dominant aqueous species of sulphur along with contours of $\log f_{S_2}$. The $\log f_{O_2}$–pH diagram was then converted into a $\log f_{O_2}$–$\log f_{S_2}$ diagram in which pH has been shown as contours of equal pH values. Stability fields of relevant ore and gangue minerals were then plotted on this diagram. All relevant reactions along with their equilibrium constants have been summarized in table 3.

The primary ores of Malanjkhand are made up of pyrite, chalcopyrite, magnetite and minor amounts of molybdenite with quartz and orthoclase as the dominant gangue minerals. Both gangue and ore minerals as discussed earlier are broadly syngenetic to each other. Sharma (1982), based on partitioning of trace elements between coexisting sulphides concluded that the ore minerals were formed in equilibrium with each other. Thus the syngenetic nature of ore and gangue mineral assemblage helps to put following limits to f_{O_2} and f_{S_2} conditions of ore deposition:

(a) Presence of molybdenite indicates that $\log f_{S_2}$ was $> -20{\cdot}65$ atm.
(b) Absence of pyrrhotite in the ores indicates that $\log f_{S_2}$ was $> -11{\cdot}6$ atm.
(c) Absence of bornite coexisting with pyrite in primary ores indicates that $\log f_{S_2}$ was $< -6{\cdot}06$ atm.
(d) Presence of equilibrium association pyrite, chalcopyrite and magnetite in ore limits f_{S_2}–f_{O_2} conditions to boundary line AB in figure 5 which is the line of coexistence of these minerals.
(e) The boundary line between orthoclase and muscovite passing along pH = 4·5 contour further narrows down the conditions towards higher pH values along the line AB, as both quartz and orthoclase, are the dominant gangue minerals in the mineralized reef. Thus, based on the above considerations the following values are obtained: $\log f_{O_2} = -34{\cdot}4$ to $-30{\cdot}2$ atm, $\log f_{S_2} = -11{\cdot}6$ to $-8{\cdot}8$ atm, pH = 4·5 to 6·5.

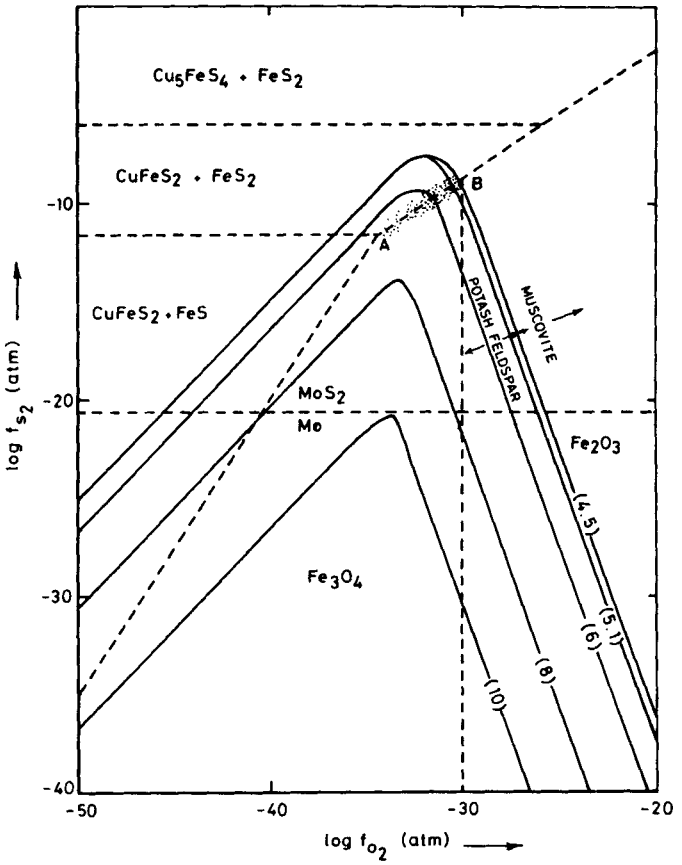

Figure 5. Log f_{S_2}–log f_{O_2} diagram showing stability fields of main minerals of primary ores from Malanjkhand. Diagram constructed for $T = 300\,^{\circ}C$, $P = 1$ atm, $\Sigma S = 0{\cdot}01$ m. —— boundaries between minerals. pH values are written in brackets. Boundary between potash feldspar and muscovite following a pH contour of 4·5 has been drawn for $K^+ = 0{\cdot}5$. Dotted area of boundary line AB represents domain of deposition of primary Malanjkhand ores.

Table 3. Equilibrium constants of relevant reactions.

Reactions	log $K_{300^{\circ}C}$
$3\,FeS + 2O_2\,(g) = Fe_3O_4 + \frac{3}{2}\,S_2\,(g)$	51·04[a]
$3\,FeS_2 + 2\,O_2\,(g) = Fe_3O_4 + 3\,S_2\,(g)$	33·60[a]
$2\,FeS_2 + \frac{3}{2}\,O_2\,(g) = Fe_2O_3 + 2\,S_2\,(g)$	27·82[a]
$4\,Fe_3O_4 + O_2\,(g) = 6\,Fe_2O_3$	30·12[a]
$FeS + \frac{1}{2}\,S_2\,(g) = FeS_2$	5·81[a]
$5\,CuFeS_2 + S_2\,(g) = Cu_5FeS_4 + 4\,FeS_2$	6·06[a]
$Mo + S_2\,(g) = MoS_2$	20·65[b]
$3\,KAl\,Si_3\,O_8 + 2\,H^+ = KAl_3\,Si_3\,O_{10}\,(OH)_2 + 6\,SiO_2 + 2\,K^+$	8·4[c]

[a]Calculated based on equations given in Ripley and Ohmoto (1977); [c]Calculated based on data from Crerar and Barnes (1976); [b]Calculated based on data in Vaughan and Craig (1978)

8. Modes of transportation and factors governing ore deposition

Freezing studies have shown that hydrothermal solutions entrapped in fluid inclusions were compositionally close to CO_2-bearing aqueous solutions of NaCl and KCl. Hence, it is logical to conclude that basic ore-forming elements were transported mainly as chloride complexes. Such a mode of transportation of ore-forming elements has since long been proved viable both theoretically as well as experimentally (Barnes 1979).

Study of fluid inclusions also revealed that quartz along with primary ore minerals was deposited from hydrothermal solutions that were boiling, leading to separation of a CO_2-rich, low-density, low-salinity fluid coexisting with a CO_2-poor fluid of higher density and salinity. Boiling has been shown to be one of the main mechanisms of ore deposition in many ore deposits particularly in copper prophyry deposits (Roedder 1984). Boiling causes cooling and increases pH of solutions making chloride complexes of ore-forming elements unstable (Barnes 1979). According to Crerar and Barnes (1976) when Fe and Cu are transported as chloride complexes, an increase of pH by one unit leads to almost total precipitation of these elements.

9. Conclusions

Fluid inclusion and mineral equilibria studies in the Malanjkhand copper deposit have indicated the following:

(i) Mineralized quartz-feldspar reef was formed from CO_2-bearing hydrothermal solutions containing appreciable amount of chlorides of sodium and potassium at temperatures between 210 and 476 °C.

(ii) Ore-forming hydrothermal solutions underwent boiling at about 307 °C, which led to the separation of a CO_2-rich fluid of low density and salinity that coexisted with another comparatively more saline and dense fluid with less amount of CO_2 (2 to 5 mol %) dissolved in it.

(iii) Pressure during entrapment from boiling hydrothermal solutions varied between 225 and 440 bars which is equivalent to a hydrostatic column depth of about 2·25 to 4·45 km or a rock depth of about 1 to 2 km respectively.

(iv) Ore-forming elements (copper, iron, molybdenum) were transported mainly in the form of their chloride complexes and boiling was the main factor which controlled ore deposition.

(v) Primary ore deposition in the reef was characterized by the following range of $\log f_{O_2} = -30{\cdot}2$ to $-34{\cdot}4$ atm., $\log f_{S_2} = -8{\cdot}8$ to $-11{\cdot}6$ atm and pH = 4·5 to 6·5.

Acknowledgements

The authors gratefully acknowledge financial support of U.G.C. under a research scheme sanctioned to S.J. We also thank Shri S.S. Subedar, and other geologists of HCL, Malanjkhand Copper Project for necessary permission and cooperation during field work. Authors also thank Dr D A Crerar and the referees for helpful comments.

References

Barnes H L 1979 *Geochemistry of hydrothermal ore deposits* (ed) H L Barnes (New York: John Wiley) p. 440
Barnes H L and Kullerud G 1961 *Econ. Geol.* **56** 648
Burruss R C 1981 *Fluid inclusions: Applications to petrology* (eds) L S Hollister and M L Crawford (Calgary: MAC short course handbook) p. 59
Collins P L F 1979 *Econ. Geol.* **74** 1435
Crawford M L 1981 *Fluid inclusions: Applications to petrology* (eds) L S Hollister and M L Crawford (Calgary: MAC short course handbook), p. 75
Crerar D A and Barnes H L 1976 *Econ. Geol.* **71** 772
Hollister L S 1981 *Fluid inclusions: Application to petrology* (eds) L S Hollister and M L Crawford (Calgary: MAC short course handbook) p. 1
Kelly W C and Turneaure F S 1970 *Econ. Geol.* **65** 609
Luckscheiter B and Morteani G 1980 *Lithos* **13** 61
MacDonald A J and Spooner E T C 1981 *Econ. Geol.* **76** 1248
Narang J L, Sharma R S, Mathur S M, Muktinath 1979 *Geol. Survey. India. Misc. Pub.* **34** 113
Ramboz C, Pichavant M, Weisbrod A 1982 *Chem. Geol.* **37** 29
Rao S K L 1974 *Indian Mineral.* **18** 28
Ripley E M and Ohmoto H 1977 *Econ. Geol.* **72** 1017
Roedder E 1963 *Econ. Geol.* **58** 167
Roedder E 1984 *Fluid inclusions* (Washington: M S A Reviews in Mineralogy 12) pp. 644
Sharma R N 1982 *Geochemistry and genesis of the copper-sulphide deposit of Malanjkhand;* Ph.D. thesis (unpublished), University of Roorkee, Roorkee
Sharma R K and Kumar R 1969 *Indian Miner.* **23** 23
Takenouchi S and Kennedy G C 1965 *Am. J. Sci.* **263** 445
Tripathi C 1979 *Geol. Sur. India Misc. Pub.* **34** 161
Vaughan D J and Craig J R 1978 *Mineral chemistry of metal sulphides* (Cambridge: University Press) pp. 493.